Strain Determination in Electrochemically Doped Single-Walled Carbon Nanotubes via Raman Spectroscopy

P. M. Rafailov,* M. Stoll, and C. Thomsen

Institut für Festkörperphysik, der Technischen Universität Berlin, Sekr. PN 5-4, Hardenbergstrasse 36, 10623 Berlin, Germany

Received: July 19, 2004; In Final Form: October 1, 2004

We studied the Raman response upon electrochemical p-doping of carbon nanotubes. The frequencies of the first- and second-order high-energy modes as excited in the range 477−780 nm were examined as a function of doping level. We relate the doping-induced shifts of selected Raman modes to the dimensional changes of the SWNTs and propose a method to determine their actuation properties from those shifts. The shift of the second-order D mode strongly depends on the excitation energy, which translates to a strong wave-vector dependence of the doping-induced shift of the phonon branches in the vicinity of the K-point of the Brillouin zone.

I. Introduction

Single-wall carbon nanotubes (SWNT) are novel one-dimensional nanostructures with promising application perspectives. Along with their remarkable electronic properties that are entirely determined by their geometry,[1] SWNTs combine large surface area, excellent chemical stability, and significant elastic properties,[2] thus appearing as appropriate candidates for novel supercapacitors,[3] batteries,[4] and actuators.[5]

Doping the nanotubes is an important method to influence their electronic and mechanical properties. Especially, electrochemical doping:charge induction by varying the potential at their contact interface with an electrolytic solution[5,8] allows a finer tuning of the added charge and hence the doping level. This is of key importance for the SWNT application as actuators, because SWNT expansion or contraction can be driven by the electrochemically induced charge; that is, a fine-tuning of the strain can be achieved. To assess the actuation properties of SWNTs, the strain must be quantified as a function of the induced charge. As one is normally interested in the strain along the nanotube axis, this can be accomplished by monitoring the tangential vibrations of SWNTs with Raman spectroscopy, because their frequencies scale linearly with doping at low doping levels.[9,10]

There are three main tangential bands in the Raman spectrum of a SWNT: the disorder-induced D mode at 1300−1400 cm^{-1}, the high-energy mode (HEM) at ∼1600 cm^{-1} with a displacement pattern derived from the E_{2g} bond-stretching mode of graphite, and the D* mode which is the second-order D mode. All of these modes were shown to originate from a double-resonance scattering mechanism involving several phonon states with relatively large wave vectors from within the Brillouin zone (BZ).[6,7] The double-resonant Raman process is a fourth-order process involving elastic scattering of the electrons by defects (or a second phonon in the second order). Thus, at a given excitation energy, the wave vector and frequency of the emitted phonon are uniquely defined by the electron and phonon dispersion relations. The resulting excitation-energy dependence of the Raman frequencies observed, for instance, for the D mode and the HEM of SWNTs is an inherent property of the double-resonant Raman scattering.

The shift of the high-energy SWNT mode (HEM) upon double-layer charging in an electrolytic solution has been intensively studied,[9−13] and for the most common laser excitation of 514.5 nm it was found to be ∼250 cm^{-1}/hole/C-atom (∼1.5 cm^{-1}/V).[9] The second-order D mode also exhibits a considerable shift upon doping.[12,14,15] From the doping-induced frequency shift, useful information on the bond length change can be obtained[10,15] as in the double-layer model the transferred charge can be calculated from the applied voltage. This is possible because of the good contact of the outer surface of SWNT-bundles with the electrolytic solution, the linear scaling of the phonon frequency with the applied voltage,[9,10] and its proven independence of the electrolyte used.[10]

However, as the HEM and the D mode are double-resonant in nature, it should be taken into account that different laser excitations will probe different regions of the bond-stretching dispersion branches, whose shift upon doping may be wave-vector dependent. Different excitation energies can thus lead to different doping-induced frequency shifts and different strain estimates for the same doping level. Here, we present a Raman investigation of the whole HEM dispersion branch by excitation-energy-dependent measurements of the HEM and the second order of the D mode of a SWNT bundle sample. We investigate the experimental conditions under which reliable strain estimates can be made and present a model for calculating the strain from the measured Raman frequency shift.

II. Experimental Section

A stripe of SWNT paper[16] with a nanotube diameter distribution ranging from 1.2 to 1.4 nm and a surface density of ∼5 × 10^{-5} g/mm^2 was prepared as a working electrode in a three-electrode cell equipped with quartz windows. The measurements were carried out using a Metrohm three-electrode potentiostat. A platinum wire and Ag/AgCl/3 M KCl served as auxiliary and reference electrode, respectively. The working electrode was dipped for its most part into the solution and was electrically

* Corresponding author. E-mail: rafailov@physik.tu-berlin.de.

10.1021/jp046803g CCC: $27.50
Published on Web 11/19/2004

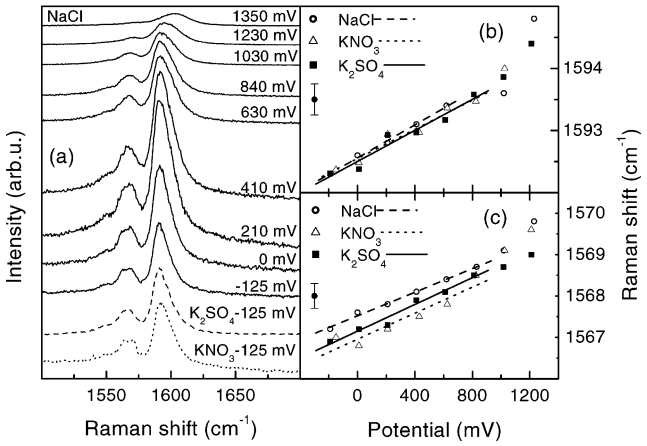

Figure 1. (a) Raman spectra at 514.5 nm excitation of the high-energy mode (HEM) at several potentials applied to the SWNT-mat in 1 M NaCl aqueous solution; lowest two traces are spectra in 1 M KNO_3 and K_2SO_4, respectively. (b) The frequency of the main HEM peak (1593 cm^{-1}) as a function of the applied potential for three different solutions: NaCl (○), KNO_3 (△), and K_2SO_4 (■). (c) Same as (b) for the second-strongest HEM peak (1567 cm^{-1}).

contacted at its dry end. At the beginning of the measurement series with each new electrolyte, the working electrode was cycled several times between 0.4 and −0.4 V in the new solution to ensure a maximum degree of wetting. Each solution was purged with N_2 gas prior to measurements to remove excessive oxygen; however, no significant changes were observed in experiments with nondeoxygenated samples. All chemicals used were of analytical grade quality. The solutions were prepared using doubly distilled water.

An Ar^+/Kr^+ laser (477, 488, 514.5, and 568 nm), a dye laser (612 nm), and a Titan-Sapphir laser (718, 738, and 780 nm) were used for excitation. The Raman spectra were recorded with a DILOR triple grating spectrometer equipped with a CCD detector. The spectrometer was calibrated in frequency using a neon lamp and the laser plasma lines.

III. Results and Discussion

We recorded the Raman spectra of the main vibrational modes from the SWNT working electrode at different constant potentials in the examined solutions (all potentials were measured vs Ag/AgCl). For three different salts (NaCl, KNO_3, and K_2SO_4) and an excitation wavelength of 514.5 nm, the recorded spectra and the phonon frequencies versus applied voltage are shown in Figure 1 for the two most intense peaks of the HEM. It was found that from −200 mV to ∼1 V, the frequency shift scales linearly with the applied potential U, that is, with the transferred charge $Q = CU$ (C being the double-layer capacitance). Furthermore, the Raman spectra measured in all solutions at the same voltage looked virtually identical, without any anion- or cation-specific differences, as exemplified for NaCl, KNO_3, and K_2SO_4 in Figure 3a for $U = -125$ mV. After comprehensive tests of our experimental conditions,[10] we were able to prove that double-layer charging is the main doping mechanism in the region from −200 mV to 1 V without a significant penetration of ionic species into the nanotube bundles. Our results therefore refer to mainly anodic polarization (p-doping) of the SWNT sample because for cathodic polarization we cannot exclude an alkali cation diffusion into the bundles even at lower negative potentials, which would comprise an onset of intercalation.[10] The double-layer capacitance was found to be ∼35 F/g by cyclic voltammetry, and the induced charge was found to be 0.005 holes/C-atom/V. Note that this kind of charge injection creates much lower doping levels than, for example, intercalation does.

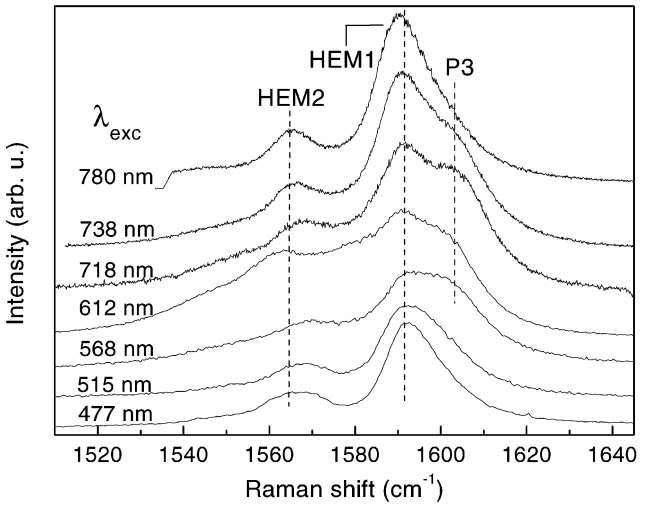

Figure 2. The HEM band as excited with various laser wavelengths at a constant doping level of $f_C \approx 0.005$ holes/C-atom ($U = 1$ V).

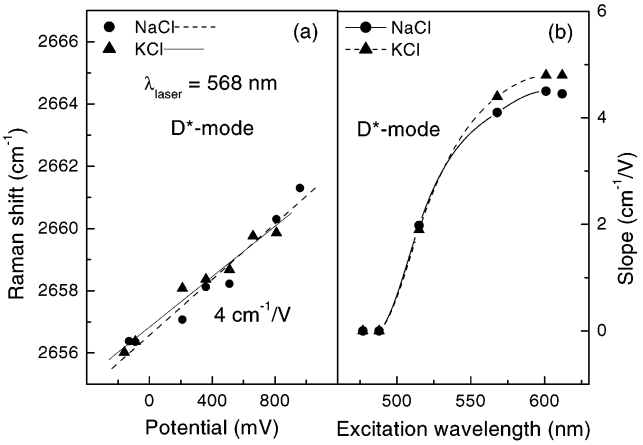

Figure 3. (a) The frequency of the D* mode as a function of the applied potential for two different solutions: NaCl (●) and KCl (▲) for $\lambda_{exc} = 568$ nm. (b) D*-mode slopes (frequency shift per 1 V vs applied potential) as obtained for various laser excitation wavelengths. The connecting lines are guides to the eye.

TABLE 1: Frequency Slopes (in cm^{-1}/V) for the RBM and HEM As Obtained from the Linear Fits within the Interval 0−800 mV (see also Figures 2 and 3)

electrolyte	HEM1: main peak	HEM2: second-strongest peak
LiCl	1.27 ± 0.12	1.54 ± 0.14
NaCl	1.33 ± 0.05	1.42 ± 0.56
KCl	1.37 ± 0.16	1.76 ± 0.11
KNO_3	1.18 ± 0.12	1.57 ± 0.28
K_2SO_4	1.25 ± 0.15	1.61 ± 0.13

From a linear fit to the frequency points in Figure 1 up to 0.8 V, we estimate an average doping-induced shift of 260 cm^{-1}/hole/C-atom (1.3 cm^{-1}/V) for the main HEM peak at 1593 cm^{-1} (HEM1) and 320 cm^{-1}/hole/C-atom (1.6 cm^{-1}/V) for the second-strongest HEM peak at 1567 cm^{-1} (HEM2), in qualitative agreement with previous results.[9] These numerical values were calculated by taking the mean value of the fitted frequency slopes for several electrolyte solutions quoted in Table 1. As can be seen from Table 1, the frequency slope of HEM2 is slightly but systematically steeper than that of HEM1. We attempted to theoretically model this slope difference by assuming an equal doping-induced upshift of the LO and TO

phonon branch in SWNT originating from the graphitic E_{2g} mode and participating in the double-resonant process to form the HEM band, LO giving rise to HEM1, and TO to HEM2.[7] These two branches have opposite slopes near the Γ point of the Brillouin zone, one dropping in energy with increasing wave vector and the other hardening and reaching an overbending. On the other hand, shifting the phonon branches to higher frequencies upon doping necessarily decreases the wave vector of the emitted phonon.[7] The hardening of HEM1 is thus weakened, while that of HEM2 is enhanced due to the different dispersion of the two branches. However, a theoretical estimate of this effect revealed a slope difference between HEM1 and HEM2 of the order 0.01 cm^{-1}/V, which lies far beyond our spectral resolution. It appears that the different slopes of HEM1 and HEM2 are really due to a different shift of the TO and LO branch[26] upon doping. We will discuss this effect again later when comparing our strain estimates to theoretical results.

Figure 2 contains Raman spectra excited at different laser energies, at a constant applied potential of 1 V. It is seen that outside the metallic resonance window (560−740 nm) the HEM band in the doped state preserves its shape consisting of HEM1 and HEM2 irrespective of the excitation energy. In contrast, upon red excitation of the doped SWNTs, we observe a qualitative change of what is known as the resonant HEM band of metallic tubes: a new peak (P3) with a still unclear origin emerges and separates from the high-frequency side of HEM1. From fitting the spectra to Voigt profiles, a shift between 3 and 4 cm^{-1}/V was established for P3. Obviously, P3 should be related to metallic SWNTs and cannot be used to describe the overall mechanical response of a charged nanotube sample. On the other hand, the peak HEM2 is very faint or missing for red laser excitation, while another peak due to metallic tube emerges at 1558 cm^{-1}. The error in the determination of peak positions is especially high for excitations in the metallic resonance window due to the broadened shape of the HEM band. Nevertheless, we found that the doping-induced shifts of HEM1 and HEM2 remain largely independent of excitation energy with more or less the same values as presented for 514.5 nm excitation, possibly due to the little dispersion of the corresponding phonon branches in the LO overbending region. Best fitting precision for these peaks was achieved at 488 nm excitation (matching the 514.5 nm results), and we argue that HEM1 and HEM2 at blue or green excitation should be used for the determination of the actuation response of SWNTs.

We further checked the doping behavior of the second-order D mode: D* (the D mode itself was too weak to be fitted reliably). With the appropriately chosen laser excitation, the D* mode exhibits a considerable shift upon doping as is seen from Figure 3a for $\lambda_{exc} = 568$ nm. However, we observe a surprisingly strong dependence of the doping-induced shift on the excitation energy: from no shift to above 4 cm^{-1}/V in going from blue to red excitation, as shown in Figure 3b.

To explain the D* mode behavior, we recall that both D and D* modes originate from phonons in the vicinity of the graphite K-point and appear in the Raman spectra due to a defect-induced double-resonant process.[6] Due to the steep dispersion of the high-energy TO phonon branch,[17] increasing the excitation energy leads to smaller wave vectors and higher frequency of the doubly resonant phonon.[6] This is illustrated in Figure 4. Doping shifts the phonon branch. This alters the double-resonance condition as only a unique pair of electronic-transition energy and phonon energy can fulfill it. Different frequency slopes of the D* mode at different excitation energies thus imply

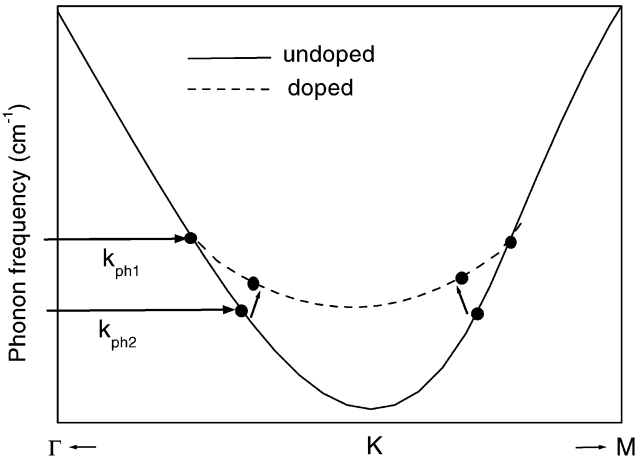

Figure 4. Phonon dispersion relation without (solid line) and with doping (dashed line) and double-resonantly excited phonon states of the D* mode (●) with their phonon wave-vectors k_{ph1} and k_{ph2}. In this example, k_{ph1} corresponds to blue excitation (no D* shift), and k_{ph2} corresponds to red excitation (maximum D* shift).

that the doping-induced shift varies with wave-vector as exemplified in Figure 4. As this variation is large and the shift can become even zero, the D* mode is unsuitable for estimates of doping-induced strain.

We must emphasize that we implicitly assume the applicability of the rigid band model in our description of doping phenomena given here; that is, we assume that doping shifts only the phonon branches and not the electronic bands themselves. At low doping levels, such an approximation is justified because of the following arguments.

Optical absorption experiments done by several research groups[8,9,18] in recent years have detected no doping-induced change in the energies of the optical transitions between van Hove singularities in SWNTs. Only once was an upshift in the first optical transition of semiconducting tubes along with bleaching reported;[9] however, this effect was attributed to the presence of different tube diameters in the sample: the corresponding bands of wide tubes are depleted/filled at lower potentials than the same bands of narrow tubes. The energies of the second "semiconducting" and the first "metallic" optical transition were found to be independent of doping even for (intercalative) doping levels 10 times higher[18] than our maximal achieved level of 0.005 holes/C-atom. At this level, the first "semiconducting" transition at most can be depleted,[18] and it is reasonable to assume that the sensitivity of the electronic bands to charge injection decreases farther away from the Fermi energy. Thus, we can conclude that the bands participating in the third "semiconducting" transition, which are relevant for 488 and 514.5 nm excitation, are quite insensitive to doping levels achievable by double layer charging.

Now, we present a simple method for calculation of the strain from the Raman frequency shift at a certain doping level. We use an elasticity-theory model previously developed to describe SWNT behavior under hydrostatic pressure.[19] The two main prerequisites that make this model transferrable to the present case are (i) the SWNT deformation upon doping is homogeneous as is the pressure-induced deformation; and (ii) the observed frequency shifts are linear in the applied voltage, similarly to the linearity in the applied pressure.

After the dynamical equation for phonon modes in the presence of strain is solved, the relative strain-induced shift of their frequencies can be obtained as

$$\frac{\omega - \omega_0}{\omega_0} = \frac{\Delta\omega}{\omega_0} = \frac{(K_{11} + K_{12})}{4\omega_0^2}(\epsilon_{\Theta\Theta} + \epsilon_{zz}) \pm \frac{1}{2}\frac{(K_{11} - K_{12})}{2\omega_0^2}(\epsilon_{\Theta\Theta} - \epsilon_{zz}) \quad (1)$$

where ω_0 (ω) is the frequency in the undoped (doped) state, and K_{ij} are tensor components describing the strain-induced change in the force constants. $\epsilon_{\Theta\Theta}$ and ϵ_{zz} are the strain components in the circumferential and axial direction, respectively. The first phonon deformation potential

$$\frac{(K_{11} + K_{12})}{4\omega_0^2} = -\gamma$$

is the Grüneisen parameter that describes the frequency shift under a fully symmetric strain. The splitting in this shift for modes vibrating in the axial and circumferential direction is caused by the shear deformation potential

$$\frac{(K_{11} - K_{12})}{2\omega_0^2}$$

The crucial difference to the high-pressure case is that upon doping a new equilibrium state of the SWNT is achieved with a minor change in the carbon−carbon bond length. This takes place by intrinsic π-orbital accommodation of the added charge, which is too small to develop significant Coulomb repulsion effects. Therefore, we argue that (i) a possible shear deformation potential should be negligibly small and (ii) the length changes of all carbon bonds are uniform, that is, $\epsilon_{\Theta\Theta} \approx \epsilon_{zz}$. The equality of axial and circumferential strain is only valid if one neglects the nanotube curvature, and this appears to be the crudest approximation we have to make. Typical examples for curvature effects in undoped SWNTs are curvature-induced energy gaps of ~0.01 eV in quasimetallic SWNTs[20] and the curvature-induced 2% softening, as compared to graphite, of the high-energy phonon branches in SWNTs in the overbending region of graphite.[21] These examples imply that curvature effects in undoped nanotubes could be neglected in many cases. However, just at low doping levels the interplay of curvature and chirality may cause deviations in axial and circumferential strain.[22] Assuming $\epsilon_{zz} = \epsilon_{\Theta\Theta}$ in eq 1 eventually reveals a simple equation for the doping-induced axial strain at a doping level f_C:

$$\frac{\Delta\omega(f_C)}{\omega_0} = -2\gamma\epsilon_{zz} \quad (2)$$

To determine the appropriate γ value, we use results on the lattice deformation in graphitic intercalation compounds (GIC). In various GICs, the in-plane expansion/contraction ϵ_{ii} of the graphite lattice was directly measured by X-ray diffraction or neutron scattering as a function of the doping level f_C. This strain scales to a good approximation linearly with doping even at the higher doping levels characteristic for GICs, and hence we can determine γ independently from our Raman measurements using the known frequency shift at our maximal doping level of 0.005 holes/C-atom. From the results presented in the literature, we could estimate:

(i) $\epsilon_{ii} = -0.085 f_C$ (X-ray diffraction on AsF_5 p-doped graphite[23]) and $\gamma = 1.07$;

(ii) $\epsilon_{ii} = -0.08 f_C$ (neutron scattering on H_2SO_4 p-doped graphite[24]) and $\gamma = 1.12$; and

(iii) $\epsilon_{ii} = -0.07 f_C$ (extrapolation of X-ray diffraction results on potassium n-doped graphite[25]) and $\gamma = 1.28$.

On the other hand, from theoretical estimations of the strain in GICs and charged graphene,[27] it follows that $\epsilon_{ii} = -0.04\%$ at $f_C = 0.005$, which again leads to $\epsilon_{ii} = 0.08 f_C$ and $\gamma = 1.12$. On the basis of these estimates, we conclude that $\gamma \approx 1.1$ is an appropriate value for the phonon deformation potential γ. Note that the fractional frequency shift $\Delta\omega/\omega$ is then only proportional to but not equal to the strain. Taking $\Delta\omega/\omega$ equal to the fractional length change of the nanotube[15] may thus overestimate the actual strain in SWNTs.

Using eq 2 with $\Delta\omega \approx 1.4$ cm^{-1} at 1 V applied potential (doping level $f_C \approx 0.005$ holes/C-atom[10]), we obtain $\epsilon_{zz} \approx -0.04\%$. For $\Delta\omega$ here, the average shift of HEM1 and HEM2 was taken as calculated from Table 1. In a recent theoretical study, the actuation response upon doping of SWNTs was examined[22] and significant chirality-dependent deviations were found. Especially, as curvature strongly modulates the character of some orbitals in semiconducting SWNTs, even at very small doping levels, they undergo strongly anisotropic deformations imitating a large shear strain that oscillates as a function of $n - m$[22] [(n,m) being the nanotube indices]. However, assuming a uniform distribution of chiralities, the average strain of a nanotube in a real SWNT sample at 0.005 holes/C-atom is about −0.035% as read out from Figure 2 of ref 22, in very good agreement with our estimate. Our value compares also very well with ab initio results for SWNTs of different diameters.[27,28] It must be stressed that due to the neglection of curvature effects our method allows one to determine only the overall actuation behavior of real nanotube samples where the theoretically predicted large oscillations in the doping-induced strain and apparent large shear strains in individual SWNTs[22] average out and the observed response is more graphite-like.

In trying to understand the difference in the shifts of the TO and LO branch[26] upon doping, we focus on eq 11 in ref 22 where analytical expressions for the SWNT strain in axial and circumferential direction are given. These expressions contain two terms that are similar for both strain types: one proportional to the modulation of the second nearest-neighbor interaction upon doping, the other being a function of the chiral angle. The circumferential strain has the additional term

$$\pm\frac{4\alpha|q|\delta n}{3KD}$$

where the plus/minus signs correspond to electron/hole doping. Here, α describes the modulation of the nearest-neighbor interaction upon doping, K is the elastic constant of the C−C bond, q is given by $(n - m)$ mod 3, D is the nanotube diameter, and δn is the transferred charge per C-atom. The D^{-1} dependence of this term implies that this is again a curvature effect that cannot be accounted for by our model which predicts equal LO- and TO-shifts. For hole doping, this term leads to a decrease of the average circumferential strain as compared to the axial one. It appears that the C−C bond perpendicular to the axis in semiconducting SWNTs becomes stiffer upon doping, which may lead to a stronger upshift of the TO-branch in these tubes, resulting in a higher effective slope for the HEM2 peak in the Raman spectra.

IV. Conclusions

We performed a Raman investigation of the high-energy modes of SWNTs upon electrochemical doping with excitation energies extending over the whole visible region (477−780 nm). We introduced a simple model by means of which the actuation

properties of carbon nanotubes can be estimated from the doping-induced shift of the high-energy graphite-like mode (HEM) and investigated the most reliable experimental conditions for such an estimate. The HEM shift should be used at higher-energy excitations where the metallic tubes are not resonant. The doping-induced shift of the D* mode was found to be strongly *k*-vector dependent and thus unsuitable for strain estimates. This leads us to conclude that the *k*-vector dependence of the doping-induced shift is stronger in those regions of the Brillouin zone where the phonon branches are more dispersive.

Acknowledgment. We gratefully acknowledge W. Frenzel for his help with the electrochemical measurements and S. Reich and J. Maultzsch for fruitful discussions.

References and Notes

(1) Rao, A. M.; Richter, E.; Bandow, S.; Chase, B.; Eklund, P. C.; Williams, K. A.; Fang, S.; Subbaswamy, K. R.; Menon, M.; Thess, A.; Smalley, R. E.; Dresselhaus, G.; Dresselhaus, M. S. *Science* **1997**, *275*, 187.

(2) Thomsen, C.; Reich, S.; Jantoljak, H.; Loa, I.; Syassen, K.; Burghard, M.; Duesberg, G. S.; Roth, S. *Appl. Phys. A: Mater. Sci. Process.* **1999**, *69A*, 309.

(3) Liu, C.; Bard, A. J.; Wudl, F.; Weitz, I.; Heath, J. R. *Electrochem. Solid-State Lett.* **1999**, *2*, 577.

(4) Claye, A. S.; Fisher, J. E.; Huffman, C. B.; Rinzler, A. G.; Smalley, R. E. *J. Electrochem. Soc.* **2000**, *147*, 2845.

(5) Baughman, R. H.; Cui, Ch.; Zakhidov, A. A.; Iqbal, Z.; Barisci, J. N.; Spinks, G. M.; Wallace, G. G.; Mazzoldi, A.; De Rossi, D.; Rinzler, A. G.; Jaschinski, O.; Roth, S.; Kertesz, M. *Science* **1999**, *284*, 1340.

(6) Maultzsch, J.; Reich, S.; Thomsen, C. *Phys. Rev. B* **2002**, *64*, R121407.

(7) Maultzsch, J.; Reich, S.; Thomsen, C. *Phys. Rev. B* **2002**, *65*, 233402.

(8) Kavan, L.; Rapta, P.; Dunsch, L. *Chem. Phys. Lett.* **2000**, *328*, 363.

(9) Kavan, L.; Rapta, P.; Dunsch, L.; Bronikowski, M. J.; Willis, P.; Smalley, R. *J. Phys. Chem. B* **2001**, *105*, 10764.

(10) Stoll, M.; Rafailov, P. M.; Frenzel, W.; Thomsen, C. *Chem. Phys. Lett.* **2003**, *375*, 625.

(11) An, C. P.; Vardeny, Z. V.; Iqbal, Z.; Spinks, G. M.; Baughman, R. H.; Zakhidov, A. A. *Synth. Met.* **2001**, *116*, 411.

(12) Corio, P.; Santos, P. S.; Brar, V. W.; Samsonidze, Ge. G.; Chou, S. G.; Dresselhaus, M. S. *Chem. Phys. Lett.* **2003**, *370*, 675.

(13) Corio, P.; Jorio, A.; Demir, N.; Dresselhaus, M. S. *Chem. Phys. Lett.* **2004**, *392*, 396.

(14) Rafailov, P. M.; Stoll, M.; Maultzsch, J.; Thomsen, C. In *Molecular Nanostructures*; Kuzmany, H., Mehring, M., Roth, S., Fink, J., Eds.; AIP: New York, 2004; p 153.

(15) Gupta, S.; Hughes, M.; Windle, A. H.; Robertson, J. *J. Appl. Phys.* **2004**, *95*, 2038.

(16) Free-standing nanotube paper (mean diameter 1.3 nm) was prepared by Roth, S., Dettlaff, U., MPI − Stuttgart.

(17) Maultzsch, J.; Reich, S.; Thomsen, C. *Phys. Rev. Lett.* **2004**, *92*, 075501.

(18) Kazaoui, S.; Minami, N.; Jacquemin, R. *Phys. Rev. B* **1999**, *60*, 13339.

(19) Reich, S.; Jantoljak, H.; Thomsen, C. *Phys. Rev. B* **2000**, *61*, R13389.

(20) Kane, C. L.; Mele, E. J. *Phys. Rev. Lett.* **1997**, *78*, 1932.

(21) Thomsen, C. *Phys. Rev. B* **1999**, *61*, 4542.

(22) Gartstein, Y. N.; Zakhidov, A. A.; Baughman, R. H. *Phys. Rev. Lett.* **2002**, *89*, 045503.

(23) Markiewicz, R. S.; Kasper, J. S.; Interrante, L. V. *Synth. Met.* **1980**, *2*, 363.

(24) Chan, C. T.; Kamitakahara, W. A.; Ho, K. M.; Eklund, P. C. *Phys. Rev. Lett.* **1987**, *58*, 1528.

(25) Nixon, D. E.; Parry, G. S. *J. Phys. C: Solid State Phys.* **1969**, *2*, 1732.

(26) In using the notations LO and TO, we mean phonons with a vibrational pattern predominantly along the nanotube axis or circumference, respectively. Note that purely axial and circumferential vibrations can exist only in armchair and zigzag nanotubes.

(27) Sun, G.; Kürti, J.; Kertesz, M.; Baughman, R. H. *J. Am. Chem. Soc.* **2002**, *124*, 15076.

(28) Sun, G.; Kürti, J.; Kertesz, M.; Baughman, R. H. *J. Phys. Chem. B* **2003**, *107*, 6924.